PCCP

PAPER

Cite this: *Phys. Chem. Chem. Phys.*, 2024, **26**, 15032

On the nature of sub-THz continuum absorption in CO_2 gas, its mixture with Ar, and in pure water vapor

T. A. Galanina,[a] A. O. Koroleva,[a] I. S. Amerkhanov,[a] E. A. Serov,[a] M. A. Koshelev,[a] M. Yu. Tretyakov,*[a] D. N. Chistikov,[abcd] A. A. Finenko[acd] and A. A. Vigasin[ab]

Received 18th January 2024,
Accepted 24th April 2024

DOI: 10.1039/d4cp00240g

rsc.li/pccp

Detailed analysis of the unique broadband millimeter-wave (70–360 GHz) collision-induced absorption spectra in pure CO_2 and in its mixture with Ar is presented. The nature of the observed continuum absorption is examined using classical trajectory simulation along with statistical physics consideration. Bimolecular continuum is decomposed in the phase space into separate contributions from the so-called free, quasibound, and true bound molecular pairs, the proportions of which greatly vary with temperature. This partitioning is supported by consideration of the second virial coefficient and excluded volume in pure CO_2, Ar, and CO_2–Ar. Close similarity between collision-induced absorption in the CO_2 containing gases and the water vapor continuum in the subterahertz spectral range is demonstrated. This similarity suggests that the physical principles underlying both continuum absorption phenomena have much in common and, therefore, can be used for continuum modeling.

1 Introduction

Precise knowledge of the continuum-like absorption of radiation by water vapor and other atmospheric gases is increasingly demanded by the most advanced climate and radiation models relevant to the Earth's, planetary, or even exoplanetary atmospheres.[1,2] It is generally accepted that continuum absorption in gases arises due to weak intermolecular interactions. Triple collisions are expected to manifest themselves at extreme gas density, which is not typical for the majority of actually known natural atmospheres. Worth mentioning is, however, that conditions in the low Venusian troposphere exemplify the case in which the consideration of only binary intermolecular interactions might become insufficient. In terrestrial-like atmospheres, the continuum is certainly caused by pairwise molecular interactions, which can manifest themselves in terms of pair collisions or in the form of some sort of van der Waals or hydrogen-bonded dimers. An assumption of only binary intermolecular interactions permits a recourse to the presently very precise quantum chemical description of potential and dipole properties characterizing weak interaction in a pair of neutral molecules.[3]

The most important example of continuum absorption in the Earths atmosphere is related to water vapor, which plays the major role in the planetary greenhouse warming effect. Interestingly, the first observation of the water vapor continuum dates back to the end of the 19th – beginning of the 20th century.[4] This effect was later interpreted in terms of an excess absorption accumulated from the far-wings of the sharp absorption lines of atmospheric molecules (resonant absorption).[5] Up-to-now, the measured continuum is determined empirically as the difference between the total observed and calculated resonant absorption of individual molecular lines. Integrated unimolecular absorption intensity varies linearly as a function of gas density. In contrast, the absorption intensity by molecular pairs, either in the course of collisional impact or in the form of a binary complex occurring in pure gases, must have a clear quadratic density dependence (being proportional to the product of partial densities in a mixture of gases). Statistical physics consideration permits distinguishing between various types of molecular pairs which can form in a gas, namely, free pairs, stable (true bound), and metastable (quasibound) dimers.[6–8] Because of the typically low interaction energy between neutral molecules, a plethora of the above-mentioned intermolecular pair states is populated at atmospheric temperatures. Consequently, one has to deal with a vast ensemble of molecular pairs, each of which is characterized by its individual absorbing features. The observed continuum then comes as a result of

[a] *A. V. Gaponov-Grekhov Institute of Applied Physics of the Russian Academy of Sciences, 46 Ulyanov str., Nyzhny Novgorod 603950, Russia. E-mail: odintsova@ipfran.ru*
[b] *A. M. Obukhov Institute of Atmospheric Physics, Russian Academy of Sciences, 3 Pyzhevsky Per., Moscow 119017, Russia*
[c] *Department of Chemistry, Lomonosov Moscow State University, GSP-1, 1-3 Leninskiye Gory, Moscow 119991, Russia*
[d] *Institute of Quantum Physics, Irkutsk National Research Technical University, 83 Lermontov str., Irkutsk 664074, Russia*

thermal averaging over a complete statistical ensemble of molecular pairs. Despite huge theoretical efforts, the impact of pair interactions on the shape of the resonant absorption line wings is still poorly understood. Its continuum-related manifestation is evaluated as the difference between the observed shape of a collision-broadened line in the region of the intermediate and far wings and the theoretical line shape, derived in the impact approximation (the Lorentz profile or its modifications).[9]

Three classes of theoretical methods have been explored in recent years aimed at simulating continuum-like spectra of atmospheric molecules without recourse to empirical parameters. These are: direct quantum mechanical (DQM) calculations, classical molecular dynamics simulation (CMDS), and classical trajectory-based simulation (CTS). These methods are capable, although to a different extent, of using *ab initio* calculated pair interaction potential and induced dipole moment. Quantum chemical calculations are presently the most accurate tool to describe intermolecular properties, utilizing an actually affordable processor time. The DQM spectra simulation, which comprises the solution to the complete scattering problem, requires significantly more computational effort than just a quantum-chemical examination of the electronic energy surface. That is why the DQM spectral simulation has been realized only for the interacting diatomics.[10,11] The CMDS method[12–14] is also heavily time- and resource-consuming and has its limitations due to the inherent approximations. In particular, taking into account only pairwise interactions in a mixture of thousands of molecules makes it difficult to properly reproduce the effect of true dimer formation. To date, this effect has only been assessed with CMDS for rare gas diatomics.[14] The CTS method[15–17] requires significantly less computational resources than the other mentioned approaches. It permits analysing the totality of the phase space of interacting monomers so that the spectra of true bound dimers can be easily reproduced. Satisfactory agreement between calculated and measured collision-induced spectra was reached using CTS in a series of simulations for various polyatomic systems, such as N_2–N_2, CO_2–Ar, CH_4–N_2.[16–21] Note, however, that both classical methods, CMDS and CTS, have to cautiously incorporate an approximate quantum correction to the spectral profile owed to the detailed balance principle.[22]

Experimental investigation of the water vapor continuum has long been a matter of paramount concern because of the exceptional role the continuum plays in the Earth's atmospheric radiation balance. Such studies are very complicated because the water vapor continuum is observed against the background of the resonant absorption, the maxima of which exceed the continuum by many orders of magnitude. At the same time, in the microwindows between monomer lines, the continuum can be an order of magnitude greater than the resonant absorption. The magnitude of the empirically determined continuum depends on the method of calculating the resonant absorption. For atmospheric applications, the continuum is usually taken into account using models largely based on available experimental data. Nowadays, the most popular and only global semi-empirical continuum model is MT_CKD.[23,24] It yields the values of a continuum in the entire range of electromagnetic waves significant for the Earth radiation balance (from 0 to 20 000 cm^{-1}). The model includes (i) the so-called "weak interaction term" which, in the opinion of the authors of ref. 23, is responsible for the continuum within the H_2O monomer vibrational-rotational bands and (ii) the term responsible for the difference in the shape of lines from the Lorentz profile in the region of the far wings, which manifests itself in the atmospheric transparency windows between the bands. The empirical coefficients of the terms are updated as new experimental data become available. An obvious drawback of the model is its inherent inability to fully take into account water dimers, whose spectral bands do not coincide with monomer bands.[25,26] In order to correctly model the continuum, it is necessary to construct a physically well-grounded model.

Carbon dioxide exemplifies another type of greenhouse gas, the continuum absorption of which has attracted much attention in recent years. Besides its significant impact on present-day terrestrial climate changes, carbon dioxide gas is a determinant for the radiative properties of Martian and Venusian atmospheres, in which its abundance absolutely dominates. Moreover, the theoretical reconstruction of paleoclimate[2,27,28] provided evidence of the critical importance of the carbon dioxide continuum absorption under the conditions characteristic of the early stages of the Earth-like planets' history. In particular, the continuum caused by CO_2 and its admixtures was pointed out to be a cause of an increase in the temperature of the early Mars atmosphere, which would have been required to keep the surface temperature above the freezing point of water.

In contrast to the H_2O molecule, the linear and centrosymmetric CO_2 molecule has no permanent dipole. Its absorption spectrum is thus incomparably simpler than that of the H_2O molecule, which makes the CO_2 molecule a nearly ideal candidate for the theoretical study of a continuum. In the case of CO_2, the mm-wave continuum absorption arises in the spectral range in which no electric dipole-permitted lines of an individual CO_2 molecule can be observed. Almost structureless collision-induced absorption bands were observed in the infrared spectra of pressurized CO_2, *e.g.*, in ref. 29–31 as well as in the millimeter (mm) wavelength range in ref. 20 (see also the references therein). The spectra of the carbon dioxide dimers and mixed bimolecular complexes were thoroughly studied in molecular beams and free jet expansions, *e.g.*, in ref. 32–34.

The present paper aims at a comparative analysis of continuum absorption in water vapor and carbon dioxide gas. We rely primarily on experimental results gained from extremely sensitive microwave spectroscopy in the sub-terahertz range. From the theoretical perspective, we use the CTS results from ref. 18 to analyze the continuum in pure CO_2 and mixture of CO_2 with Ar (supplemented here with detailed decomposition of bimolecular absorption) as well as the results of quantum mechanical calculations of the water dimer spectrum.[35] It should be noted that the results obtained in ref. 18 and 35 are among the most elaborated in terms of their accuracy and spectral coverage. It is worth noting that the spectral range under consideration is being actively explored by radiometric methods in the interests of remote sensing of the Earth's atmosphere,[36] for which physically well-grounded modeling is highly desirable.

To analyze the water vapor continuum, we used presumably all available experimental data known from the literature. For pure CO_2 and for a mixture of CO_2 with Ar, we carried out additional measurements in a very wide range of frequencies (70–360 GHz) and temperatures (268–332 K), complementing and validating the previous studies (see ref. 20 and references therein). Independent verification of experimental data is necessary because there are numerous cases where repeated measurements of weak continuum absorption do not agree with the previous ones within stated errors.[37–46] The new experimental data obtained in the present work are characterized by: (i) extension of the explored wavelength range, including the long-wavelength region, in which, according to our calculations, the maximum of the spectral function relevant to CO_2–Ar dimers should be observed, and (ii) examination of the temperature dependence of the continuum.

It should be pointed out that detailed experimental data on the continuum absorption in CO_2–CO_2 and CO_2–Ar systems are needed for validating the CTS results,[18] which we believe to be a promising tool for subsequent simulation of the atmospheric continuum.

2 Experimental details

The continuum absorption spectra were investigated following the approach used in our previous works.[19,20] The absorption coefficient $\alpha(f)$ was obtained with a resonator spectrometer,[47,48] the operating principle of which is based on measuring changes in the resonance curve width of a high-finesse (quality factor $Q = f/\Delta f \sim 10^6$) Fabry–Perot resonator filled with absorbing gas:

$$\alpha(f) = \frac{2\pi}{c}(\Delta f - \Delta f_0), \quad (1)$$

where f is the resonance frequency, c is the speed of light, Δf and Δf_0 are the widths of the resonance curve when the resonator is filled with the investigated (absorbing) and non-absorbing gases, respectively. Absorption measurements are carried out at TEM00q frequencies of the cavity modes separated from each other by approximately 300 MHz. As a radiation source, we use backward wave oscillators (BWO) OB-71 (70–120 GHz), OB-76 (105–148 GHz), OB-24 (155–255 GHz), and OB-30 (247–357 GHz) stabilized using a phase-locked loop (PLL) system against the harmonic of a microwave synthesizer.

The resonator is located vertically inside a thermally stabilized gas chamber, and the temperature is maintained constant by an active regulated thermostat. The absorption is measured at pressures up to 2 atmospheres and temperatures ranging from 268 to 332 K.

The experimental procedure was described in detail in ref. 20, where the continuum was reported for pure CO_2 and its mixture with Ar at room temperature in the frequency range of 105–240 GHz. To determine the resonator losses (instrumental baseline), the widths of the resonance curves are measured when the chamber is filled with Kr (for pure CO_2) and Ar (for CO_2–Ar mixture). We use samples of CO_2, Ar, and Kr gases with purity declared by the manufacturer better than 99.99%. Gas pressure is continuously monitored by a pair of Baratron sensors with upper limits of 1000 and 2000 Torr with 0.25% reading accuracy, as stated by the manufacturer. The temperature of the gas and resonator mirrors is continuously monitored by Pt100 platinum sensors (the sensor error in the temperature range under study does not exceed 0.2 K). Gas temperature sensors are located near each mirror and in the middle between them. The difference in the gas temperature inside the resonator ranged from 0.15 K (at 297 K) to 5.1 K (at 268 K). The efficient gas temperature is calculated as the average value of the temperature height profile (the integral of the temperature distribution over height normalized to the resonator length). The difference between the average temperature and the arithmetic mean ranged from 0.1 K (at 297 K) to 1.1 K (at 333 K). The experimental conditions are listed in Table 1.

3 Determination of the continuum

The experimentally measured continuum absorption coefficient α consists of the absorption due to the interaction of CO_2 molecules with each other (self-continuum) and with Ar molecules (foreign-continuum):

$$\alpha = \alpha_{CO_2\text{–}CO_2} + \alpha_{CO_2\text{–}Ar}. \quad (2)$$

In the case of pure CO_2 gas, the second term in eqn (2) is zero. To determine the bimolecular absorption coefficient of CO_2–Ar from eqn (2) we used a smooth function approximating the CO_2–CO_2 experimental data (see eqn (4) below). The value of bimolecular absorption is proportional to the product of the concentrations of interacting molecules:

$$\alpha_{X-Y}(f,T,n) = C_{X-Y}(f,T)n_X n_Y = \left(\frac{f}{c}\right)^2 S_{X-Y}(f,T)n_X n_Y, \quad (3)$$

where X and Y denote the molecules, n is the concentration of the molecules, T is temperature, C is the absorption coefficient normalized to the concentrations, and S is the reduced spectral

Table 1 Experimental conditions

	CO_2–CO_2				CO_2–Ar			
Frequency range, GHz	70–120	105–145	157–255	247–357	70–120	105–145	157–255	247–357
Temperature, K	297	268–317	268–332	297	297	268–317	268–317	297
Pressure, Torr	1310	750–1250	1000	1300	1295	900–1400	1200	1300
CO_2 content, %	100	100	100	100	31	18–33	34	31
Number of recordings	6	18	10	2	6	16	18	6

function (hereafter called just the spectral function for brevity). The spectral function corresponds to the normalization of the coefficient C by the radiation term common for all absorbers, which is equivalent to the frequency squared in the subTHz frequency range. The use of the spectral function is convenient when considering the continuum in the subTHz range, as it reflects the individual characteristics of the molecular spectra.

3.1 Frequency dependence of the CO_2–CO_2 and CO_2–Ar continuum

The experimental data on the spectral functions of CO_2–CO_2 and CO_2–Ar in the frequency range from 70 to 357 GHz at a temperature of 297.3(2) K are presented in Fig. 1 and 2, respectively. A notable increase of experimental noise in the low frequency part of the range is caused by the data normalization by the frequency squared. Combined with our previous measurements,[20] the new data continuously covers the frequency range under consideration. The original absorption spectra were recorded step by step (independently for each of the four sub-bands corresponding to the operating frequency range of the BWOs, and the radiation source change is accompanied by a simultaneous replacement of all elements of the waveguide path, including the detector). Thus, the agreement between the data obtained in different sub-bands indicates their reliability.

It is worth noting that the value of the CO_2–Ar continuum (and, therefore, the signal-to-noise ratio in the spectrum recording) is 3–4 times less than that for the CO_2–CO_2 continuum. Considering the fact that significant variation of the

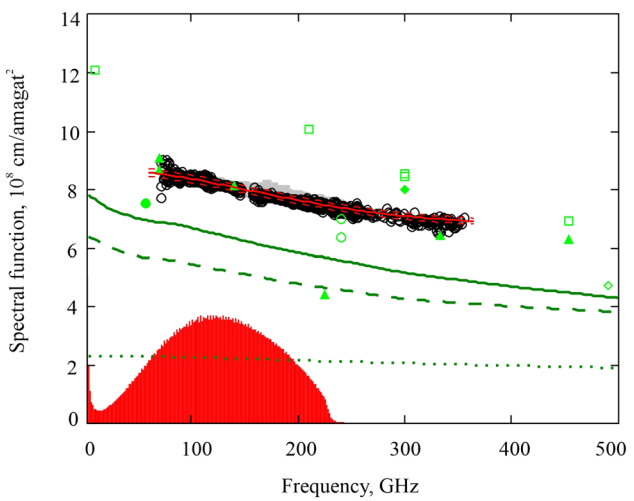

Fig. 1 Spectral function of the CO_2–CO_2 continuum at 297 K: new experimental data (black symbols), experimental data[20] (gray symbols), experimental data[49,52–54,56–60] (green symbols), approximation of new experimental data by function (4) (red solid curve) together with the total uncertainty of the approximation (red dashed curves), result of calculation of bimolecular absorption (free pairs, stable and metastable dimers)[18] – green solid curve, the result of calculating absorption by free molecular pairs and metastable dimers[18] (green dashed curve), the result of calculating absorption by free molecular pairs only (green dotted line). Red vertical bars are the CO_2–CO_2 rigid rotor spectrum stick-diagram (see text for details).

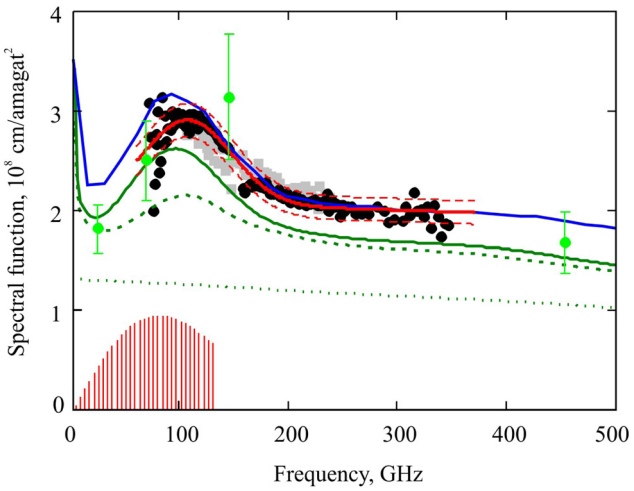

Fig. 2 Spectral function of the CO_2–Ar continuum at 297 K: new experimental data (black symbols); experimental data from ref. 20 (gray symbols); approximation of experimental data by function (4) (red solid curve) together with the complete uncertainty of the approximation (red dashed curves); experimental data[49–51] (bright green symbols); calculated bimolecular absorption[18] for free pairs (green dotted curve), free pairs and metastable dimers (green dashed curve), free pairs, stable and metastable dimers (solid green curve); calculated bimolecular absorption (free pairs, stable and metastable dimers)[16] (blue solid curve). Red vertical bars are the CO_2–Ar rigid rotor spectrum stick-diagram (see text for details).

CO_2–Ar spectral function occurs in frequency intervals much larger than the frequency step corresponding to the free spectral range of the cavity, the obtained data were averaged over five neighboring frequency points. A similar procedure was applied to our previous data[20] for adequate comparison.

The whole set of experimental data on spectral functions for pure CO_2 and its mixture with Ar were approximated by a function, the shape of which was empirically determined from the results of numerical CTS:

$$F(f,T) = a_0\left(1 - a_1 f^2\right) + a_2 \exp\left(-\frac{(f-a_3)^2}{{a_4}^2}\right), \qquad (4)$$

where a_i are numerical parameters, some of which depend on temperature (these dependences will be discussed in the next section).

The uncertainty of the fitted spectral functions consists of statistical uncertainty (experimental noise) as well as uncertainty in measuring gas temperature and pressure and inaccuracy in determining the contribution of continuum absorption of water vapor, which is an inevitable microimpurity of investigated gases ever present in the spectrometer chamber. The resulting uncertainty of the spectral function, defined as the square root of the sum of all the listed uncertainties squared, is 1.6% and 5.9% for $S_{CO_2\text{–}CO_2}(f)$ and $S_{CO_2\text{–}Ar}(f)$, respectively. Note that the uncertainty of $S_{CO_2\text{–}Ar}(f)$ also includes the uncertainty of $S_{CO_2\text{–}CO_2}(f)$ (see details in Appendix A).

The experimental data from the literature[49–58] and the results of calculations of bimolecular absorption by the CTS method[16,18,20] are presented in Fig. 1 and 2 for comparison.

In the case of the CO_2–CO_2 continuum, the uncertainty is unknown for most experimental data from the literature, but their scatter indicates greater uncertainty compared to our results. Taking this into account, the new data on the CO_2–CO_2 continuum are consistent with the previous results. The calculated bimolecular absorption underestimates the experimental one by approximately 24%, but well reproduces the shape of the observed frequency dependence. Considering the complexity of the object, this can be considered a good agreement.

As for the CO_2–Ar continuum, there are CTS results from two independent research groups.[16,18] The experimental data are between the two sets of the calculated values. One of them[18] underestimates the observed absorption by ~10%, and the other[16] overestimates it by ~3%. The presence of a broad peak centered around 100 GHz is observed in both the calculated and experimental spectra. The presence of the peak is also indirectly evidenced by the earlier measurements,[49–51] which show a significantly greater uncertainty (up to 20%) compared to our data.

Table 2 Parameters introduced in eqn (4) and (5) fitted to experimental data

	CO_2–CO_2	CO_2–Ar
c_0, 10^{-7} cm amagat^{-2}	6.471	0.536
d_0, 10^{-9} cm amagat^{-2} K^{-1}	−3.329	−0.1095
e_0, 10^{-12} cm amagat^{-2} K^{-2}	4.645	0
a_1, 10^{-7} cm amagat^{-2} GHz^{-2}	0	2.778
c_2, 10^{-7} cm amagat^{-2}	3.166	0.364
d_2, 10^{-9} cm amagat^{-2} K^{-1}	−1.718	−0.095
e_2, 10^{-12} cm amagat^{-2} K^{-2}	2.415	0
a_3, GHz	0	107.0
a_4, GHz	219.0	57.62

3.2 Temperature dependence of the CO_2–CO_2 and CO_2–Ar continuum

Measurements of CO_2–CO_2 and CO_2–Ar continua were carried out at temperatures ranging from 268 to 332 K in the 105–255 GHz frequency range. The expected increase in bimolecular absorption with decreasing temperature was observed. The temperature dependence of the continuum in this work was modeled using the dependence of the parameters a_0 and a_2 in the form of a polynomial:

$$a_{0,2}(T) = c_{0,2} + d_{0,2}T + e_{0,2}T^2. \quad (5)$$

The values of the parameters introduced in eqn (4) and (5) are presented in Table 2. The spectral functions for CO_2–CO_2 and CO_2–Ar, recorded at five temperatures, together with their approximations, eqn (4), are presented in Fig. 3.

The uncertainty of these spectral functions was assessed as mentioned above and does not exceed 1.8% and 4.4% for $S_{CO_2\text{–}CO_2}(f)$ and $S_{CO_2\text{–}Ar}(f)$, respectively (see details in Appendix A). The systematic difference between the results of our experiments and the CTS of bimolecular absorption for CO_2–CO_2 and CO_2–Ar for each of the considered temperatures is about 24% and 10%, respectively. This indicates that the temperature dependence of the calculated absorption coincides with the experimental one, but there is a systematic underestimation of the absorption, which manifests itself as a temperature-independent factor (see Fig. 3).

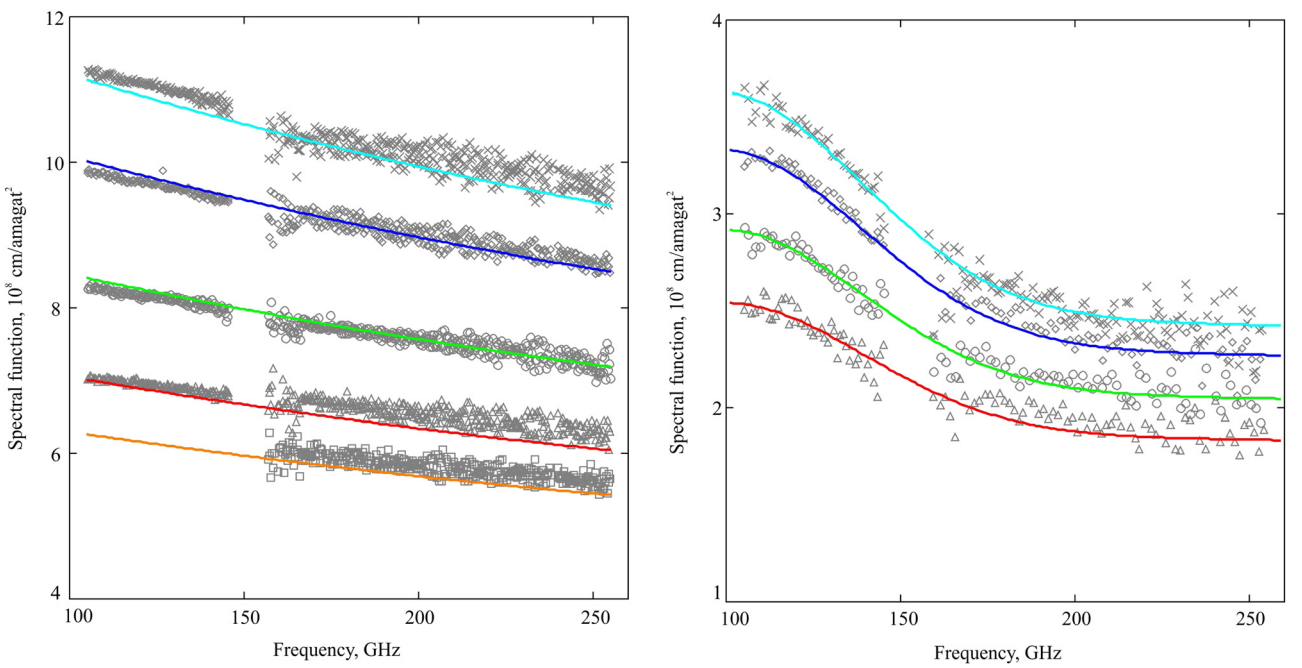

Fig. 3 Spectral function of CO_2–CO_2 (left) and CO_2–Ar (right): experimental data (different gray symbols from top to bottom at 268, 279, 297, 317 K and only for CO_2–CO_2 at 332 K) and results of CTS (solid colored curves) adjusted by eye to experimental values using arbitrary constant factors 1.24 and 1.08 for CO_2–CO_2 and CO_2–Ar, respectively (see text for details).

4 Interpretation of observed data

Classical trajectory-based simulation makes it possible to single out separate contributions of free pairs, metastable, and stable dimers from the totality of the observed bimolecular absorption (Fig. 1 and 2). It is seen that the calculated spectral functions characterizing absorption by CO_2–CO_2 and CO_2–Ar pairs behave differently. However, we can suggest that the observed decrease in the CO_2–CO_2 spectral function and a broad peak at about 100 GHz in the CO_2–Ar spectral function are caused by the absorption of stable and metastable dimers. This idea can be supported qualitatively by plotting stick diagrams of the CO_2–Ar and CO_2–CO_2 stable dimers, as shown in Fig. 1 and 2, respectively. The rightmost line on the frequency scale in each diagram corresponds to the rotational predissociation limit for each of the dimers, comprising that the rotational energy is approximately equal to the dissociation energy (166 cm^{-1} for CO_2–Ar and 392 cm^{-1} for CO_2–CO_2[61]). The rotational lines in the CO_2–Ar diagram (Fig. 2) are concentrated in the vicinity of the peak in the observed spectrum. The CO_2–CO_2 rotational spectrum (Fig. 1) is much denser, and its peak of the spectral function is significantly less pronounced. Nevertheless, we can state that the CO_2–CO_2 dimer rotational spectrum is located in the same region of the spectrum. Recall that the CO_2–CO_2 dimer has a centrosymmetric parallel-slipped structure in its ground state, hence it has no permanent dipole, which could give rise to the rotational absorption spectrum of a rigid dimer. The rotational dimeric spectrum can arise, however, provided the ground state geometry is distorted in the course of thermal excitation of true bound and, especially, quasibound dimers. The examination of the spectral functions shown in Fig. 1 and 2 suggests that the nature of the observed features should be attributed to the envelope of the rotational spectra of the respective dimers. In support of this statement, we have to remind that a quite satisfactory quantitative and qualitative agreement between our trajectory-based calculations and available observations was reached without recourse to the empirically defined parameters by accounting for the totality of intermolecular pair states. Having said this, we are confident in our claim that the nature of the observed continuum in CO_2–CO_2 and CO_2–Ar is established reliably, at least within the frequency range under consideration.

The next section supplements the above conclusion by discussing the relationship between the bimolecular absorption in CO_2–CO_2 and CO_2–Ar and the decomposition of the second virial coefficient (SVC) of pure gases and their mixture, as suggested by Storgyn and Hirschfelder.[6]

5 What can we learn by examining the SVC for pure gases and their mixture?

Let us first consider the partitioning of pair molecular states into free, quasibound, and true bound states. The absolute number of pair states is obviously diverging as a gas volume. To have converged the integrals over selected domains of states, it is reasonable to integrate the induced dipole squared, which decreases rapidly as a function of intermolecular separation. This would permit us to approximately characterize the partitioning of the integrated intensity of induced absorption rather than the partitioning of the literally said molecular pair states in a gas. On the one hand, we can use the approximate method of partitioning in kinetic energy space, first suggested in ref. 7 and then improved in ref. 8. On the other hand, we know that in the case of CO_2–Ar such partitioning was already strongly supported by a detailed examination of a vast amount of classically calculated trajectories.[62] Fig. 4 shows that, expectedly, true bound dimers largely manifest themselves at very low temperatures. The fraction of quasibound dimers cannot be neglected over a wide range of temperature. We emphasize here that the proportion of thus determined contributions at any given temperature is strongly sensitive to details of potential and dipole surfaces, including the number of intermolecular degrees of freedom. That is why we can expect that partitioning similar to that shown in Fig. 4 is qualitatively valid for two interacting water molecules, though the quantitative contributions of each group of pair states to the observed absorption will be different. More precisely, it was shown in ref. 63 and 64 that true bound and quasibound water dimers are approximately equal contributors at near-room temperature, whereas the contribution of free pairs is almost negligible.

Coming back to the studied systems, we can easily find partition functions for both true bound Q^{b}_{pair} and quasibound Q^{m}_{pair} dimers by making use of classical integration within preselected limits in the phase space.[8] Then, these partition functions, together with the monomer-progenitor partition functions Q_{mon_1} and Q_{mon_2}, can be used for evaluating the respective equilibrium constants for true bound and quasibound dimers:

$$K^{b}_{p} = \frac{1}{P}\frac{Q^{b}_{pair}}{Q_{mon_1}Q_{mon_2}}, \quad K^{m}_{p} = \frac{1}{P}\frac{Q^{m}_{pair}}{Q_{mon_1}Q_{mon_2}} \qquad (6)$$

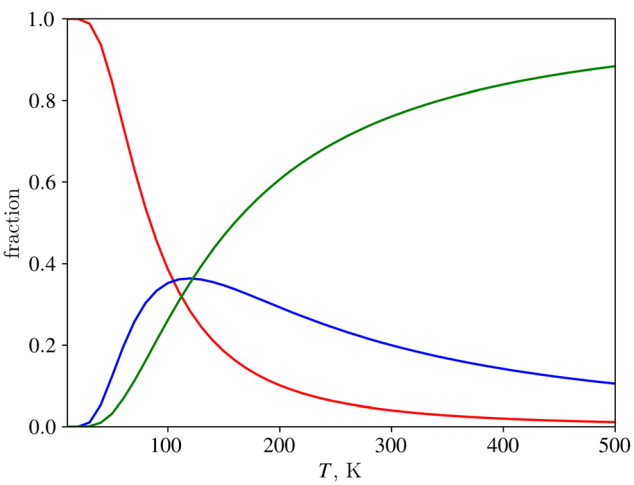

Fig. 4 Normalized contributions to CO_2–Ar integrated absorption (zeroth spectral moment) from various domains of pair states following the phase space averaging suggested in ref. 8. The fraction of free pairs is shown by green line, red and blue lines refer to true bound and quasibound dimers fractions, respectively.

as detailed in ref. 65. Armed with the knowledge of these equilibrium constants, it is tempting to examine the components of the second virial coefficient using the model described below.

Let us consider the truncated virial equation of states:

$$\frac{PV}{RT} = 1 + \frac{B}{V}. \tag{7}$$

Here, the second virial coefficient can be decomposed as[6]

$$B = B^{\mathrm{f}} + B^{\mathrm{b}} + B^{\mathrm{m}}, \tag{8}$$

in which the superscripts f, b, m are related to free, bound and metastable pairs, respectively. The term B in eqn (8) can be represented as[6]

$$B = B^{\mathrm{f}} - RTK_{\mathrm{p}}, \tag{9}$$

where K_{p} is the equilibrium constant for a homomolecular dimer, R is the gas constant, and T is the temperature. The term B^{f} can be tentatively identified with the so-called excluded volume b_0, which is conventionally defined as an empirical parameter entering the van der Waals equation of state. Then, the SVC in eqn (9) takes on the form[6]

$$B = b_0 - RTK_{\mathrm{p}} = b_0 - RT\left(K_{\mathrm{p}}^{\mathrm{b}} + K_{\mathrm{p}}^{\mathrm{m}}\right). \tag{10}$$

In the case of the mixture of two gases 1 and 2 with mole fractions x_1 and x_2, the SVC in eqn (7) is given by[6]

$$B = B_{11}{x_1}^2 + 2B_{12}x_1x_2 + B_{22}{x_2}^2, \tag{11}$$

where B_{11} and B_{22} are usual SVCs for pure gases (CO_2 and Ar in our case) and B_{12} is the mixed or cross virial (CO_2–Ar) term, which has the form[6]

$$B_{12} = B_{12}^{\mathrm{f}} - \frac{1}{2}RTK_{\mathrm{p}_{12}} = b_{0_{12}} - \frac{1}{2}RT\left(K_{\mathrm{p}_{12}}^{\mathrm{b}} + K_{\mathrm{p}_{12}}^{\mathrm{m}}\right). \tag{12}$$

Here, $K_{\mathrm{p}_{12}}$ is the equilibrium constant for a mixed 1–2 (heteromolecular) complex, which can be also either bound or metastable, and $b_{0_{12}}$ is the mixed excluded volume.

It is worth recalling here the general expression for the classical SVC which is valid for both pure gases and binary mixtures[65]

$$B^{\mathrm{class}}(T) = \pi N_{\mathrm{A}} \frac{\int\cdots\int\left(1 - \exp\left(-\frac{V(R,\Omega)}{k_{\mathrm{B}}T}\right)\right) f(\Omega)R^2\mathrm{d}R\mathrm{d}\Omega}{\int\cdots\int f(\Omega)\mathrm{d}\Omega}, \tag{13}$$

where N_{A} is the Avogadro number, k_{B} and T are the Boltzmann constant and the temperature, R and Ω are, respectively, the center of mass separation and the set of intermolecular angular coordinates defining relative orientation of the interacting monomers, $f(\Omega)$ is the angular part of the Jacobian (see, *e.g.*, ref. 66), $V(R,\Omega)$ is the interaction potential assuming that the monomers are rigid, as used for the calculations in the present work. The virial coefficients obtained in this way from the potentials used in our CTS are presented in Fig. 5 together with known experimental data demonstrating their good agreement.

Thus, the value of excluded volume can be evaluated from eqn (10) and (12) using the corresponding values of SVC and the equilibrium constants obtained from partition functions over preselected domains of phase space (Fig. 6).

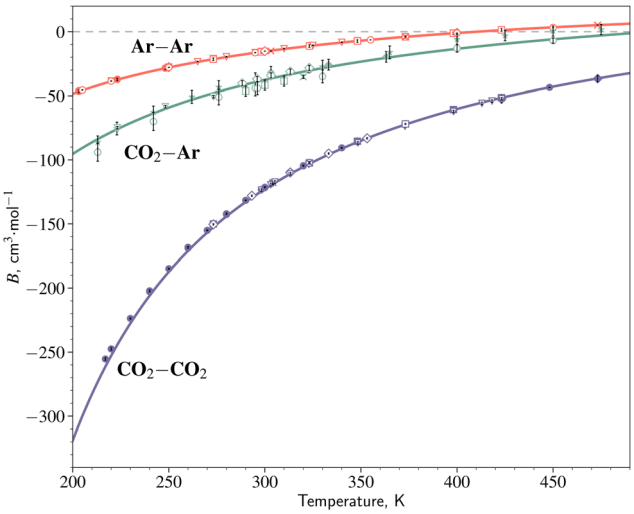

Fig. 5 Temperature variation of SVC for CO_2–Ar, CO_2–CO_2 and Ar–Ar. Solid curves show calculated SVC using eqn (13) with *ab initio* potentials. The symbols are taken from a collection of available experimental data.[67] The error bars for measured virial coefficients of pure gases are, in most cases, inferior to the symbol size.

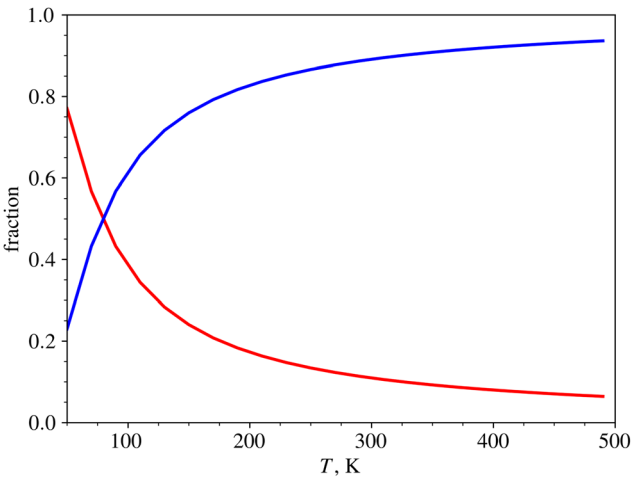

Fig. 6 Normalized partition functions of states for true bound (red trace) $Q_{\mathrm{pair}}^{\mathrm{b}}/(Q_{\mathrm{pair}}^{\mathrm{b}} + Q_{\mathrm{pair}}^{\mathrm{m}})$ and quasibound (blue trace) $Q_{\mathrm{pair}}^{\mathrm{m}}/(Q_{\mathrm{pair}}^{\mathrm{b}} + Q_{\mathrm{pair}}^{\mathrm{m}})$ dimers for CO_2–Ar *versus* temperature, calculated as suggested in ref. 8.

One has to keep in mind, however, that all values in eqn (10) and (12) are temperature-dependent, stipulating that the excluded volume also has to vary as a function of temperature.

The value of the excluded volume can be found otherwise, assuming its relation to the critical parameters stemming from the van der Waals equation of state. In this case, however, the excluded volume is constant and, thus, exhibits no temperature dependence. In the hard sphere approximation, the combination rule $b_{0_{12}} = (b_{0_{11}} + b_{0_{22}})/2$ is often used to determine the mixed excluded volume.

Fig. 7 demonstrates that, in the high temperature limit, b_0 as estimated from our calculated equilibrium constants either for pure CO_2 and Ar or for their mixture seems to converge smoothly towards the constant values derived from the van der Waals equation.

At a qualitative level, the temperature variation of b_0 (or of B^f) can be understood, noting that repulsive forces dominate in the intermolecular interaction in the high-temperature extreme. As a result, the entire SVC is largely due to B^f, which is determined by "one-touch-collisions" similar to a hard-sphere impact. Being positive, B^f can be called b_0 associated approximately with "forbidden" volume for the neighboring molecules. Fig. 4 clearly illustrates the dramatically temperature dependent partitioning among relative fractions of free, bound, and quasi-bound pairs in a gas. In the low-temperature extreme, attractive forces are obviously prevalent, thus resulting in molecular association.

It is worth noting that in a highly cooled gas the SVC is more negative than it could be, provided it is due to molecular association only. It was pointed out first in ref. 6 that at low temperatures B^f and, therefore, b_0, become negative, thus showing the limitation of the concept of excluded volume.

Finally, it should be emphasized that within the broad temperature range, the b_0 factor has no literal meaning of any kind of excluded volume, although within a limited temperature interval, b_0 is virtually constant and its value is close to the proper volume of colliding molecules. This means that any simplistically estimated b_0 should be used with great care and only within a very limited temperature range. As an example, we would like to recall the attempt to evaluate b_0 for water vapor from the distance of minimal approach in a head-on molecular collision proposed in ref. 68 and further developed in ref. 69 using a real interaction potential. The results of analogous excluded volume evaluation for the considered systems are shown in Fig. 7 for comparison.

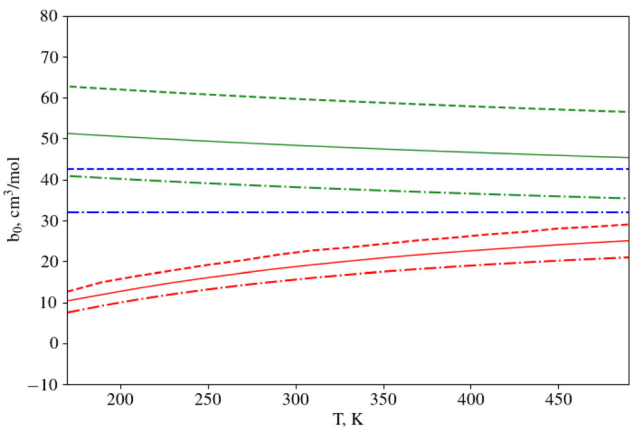

Fig. 7 Temperature variation of excluded volume b_0 for pure CO_2, Ar, and CO_2–Ar mixture. Red curves show b_0 calculated as B^f part of SVC (see eqn (10) and (12), respectively). Blue straight lines show b_0 taken from the relevant van der Waals equation of state, green curves refer to expressions suggested by Leforestier.[69] Solid curves refer to the mixture of CO_2 with Ar, dash-dotted and dashed lines refer, respectively, to pure Ar or CO_2.

6 About similarity between CO_2 and H_2O continuum

The precedent sections present thorough investigation of the CO_2–CO_2 and CO_2–Ar continuum in the spectral range where pure rotational transitions of corresponding paired molecules are located. These continua demonstrate its clear resemblance to what is observed in the water vapor continuum explored recently using the Fourier-transform technique at the AILES facility of SOLEIL synchrotron.[70–73] When considered conjointly with the previous results from ref. 47 and 74–82, these data reveal a sharp decrease in the spectral function of the H_2O–H_2O continuum in the 500–1000 GHz range (Fig. 9). It could be tentatively suggested that such a decrease is characteristic for the envelope of the H_2O dimer rotational spectrum. This decrease in spectral function is similar to variations of the CO_2–CO_2 and CO_2–Ar spectral functions in the 100–500 GHz and 100–180 GHz range, respectively, in which calculations clearly shows the manifestation of true bound and quasibound dimers (Fig. 1 and 2).

Let us illustrate in more details the suggested closeness between spectral function of considered collisional systems. Currently, the continuum absorption of water vapor cannot be calculated from the first principles, *i.e.* without recourse to adjustable parameters in view of the complexity of the object. Therefore, in ref. 73 it was proposed to use a simplified model based on the mechanisms of continuum formation, same as in CO_2–CO_2 and CO_2–Ar collisional systems. The model takes into account the absorption by metastable and stable dimers using the calculated spectrum of stable dimers[35] and equilibrium constants from ref. 78. The contribution of free pairs to the water vapor continuum is not taken into account, as it is negligibly small.[7,83] The contribution of line mixing to water vapor continuum is also neglected.[84]

In addition, the model includes the difference between the observed shape of the resonance line wings and the Lorentzian one according to the semi-empirical model proposed in ref. 9. Corresponding spectral function in the subTHz spectral range can be reduced just to the constant, which is the first variable parameter of the model.

Its second variable parameter takes into account not quite certain absorption spectrum of metastable dimers. When modeling their spectrum, two extreme cases are considered.[39,85] In the first extreme, it is assumed that a metastable dimer is a binary molecule similar to a stable dimer but having a limited lifetime. Then its spectrum can be represented as a uniformly broadened spectrum of a stable dimer. In the second extreme, a metastable dimer is thought to be similar to a pair of two monomers rotating almost freely next to each other, so that its absorption spectrum is close to the doubled spectrum of a single monomer uniformly broadened due to the short lifetime. As both these cases do not reflect all characteristics of the spectrum of a metastable dimer, it was suggested in ref. 73 to take into account its absorption in the form of a superposition of these two models. This approach implies the presence of a one-variable parameter characterizing the relative contribution of both extreme models for a metastable dimer. The continuum model fits better to the available amount of experimental data

in the subTHz range, provided the spectrum of metastable dimers is represented as the envelope of the stable dimer spectrum. This is in agreement with the conclusion derived in the course of examination of the mm-wave continuum (188–258 GHz),[78] in which a sequence of dimeric peaks is clearly seen.

In the spirit of the simplified approach employed in ref. 73, we simulated the spectral function of the metastable dimers for CO_2–Ar at near-room temperature. The shape of the spectrum of metastable pairs was found as the weighted sum of the bound and free profiles, as obtained from the CTS. The best agreement between the one-parameter model and the calculated envelope of metastable states was obtained at a relative contribution of free pair states of 35% as demonstrated in Fig. 8. We can conclude that, in the case of CO_2–Ar, the spectral function of metastable pairs strongly resembles that of the bound pairs. This conclusion is in line with what has been remarked in the paragraphs above while considering the results of the water vapor absorption in the subTHz spectral range.

The two variable parameters of the model are determined from the best fit to the experimental spectra.[47,70,73–82] These experimental data and the simulation results are presented in Fig. 9. The figure also shows a stick-diagram of the rotational spectrum of a rigid diatomic molecule with the same rotational constants as that of a water dimer (B = 6.161 GHz and D = 50 kHz[86]) taking into account the dimer dissociation energy (1105 cm^{-1} [87]).

The comparison of the obtained information about the CO_2–Ar and CO_2–CO_2 continua with the experimental data and the results of modeling the H_2O–H_2O continuum using the aforementioned simplified approach allows us to make the following

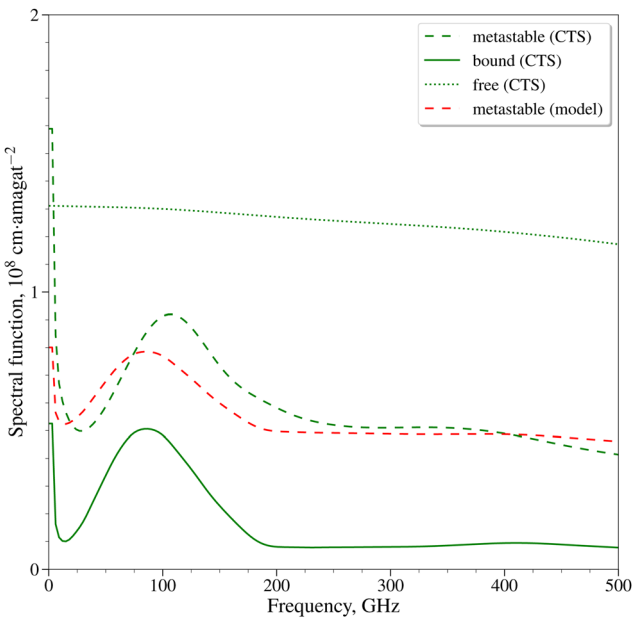

Fig. 8 The simulated spectral function of metastable states for CO_2–Ar at T = 298 K. The green dashed curve refers to the envelope resulting from the CTS calculations, and the red dashed curve shows the approximated spectrum obtained using a one-parameter model (see the discussion in the text).

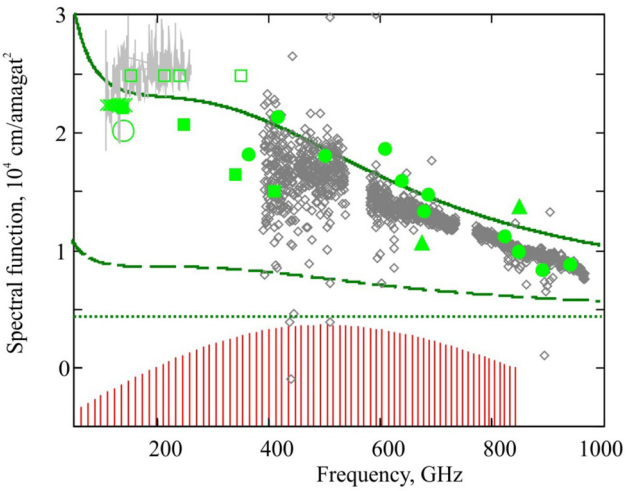

Fig. 9 Spectral function of H_2O–H_2O continuum at 296 K: experimental data from ref. 47, 73, 77 and 78 (gray) and from ref. 74–76 and 79–82 (bright green symbols), far wing model (dotted line), contribution of far wings and metastable dimers (dashed curve), total continuum model (solid curve). Stick-diagram corresponds to the end-over-end rotation of H_2O dimer (see text for details).

proposition about the nature of the continuum: (1) the observed spectral features (the peak of the spectral functions of CO_2–Ar in the range of 70–180 GHz and the decline of the spectral functions of CO_2–CO_2 and H_2O–H_2O in the ranges of 105–260 GHz and 300–1000 GHz, respectively) are due to the absorption by dimers, which confirms the fact of their existence in close to atmospheric equilibrium thermodynamic conditions and their significant contribution to the observed continuum; (2) in addition to dimers, free pairs make a substantial contribution to the CO_2–Ar and CO_2–CO_2 continua; they can be neglected for the H_2O–H_2O continuum, but the manifestation of super-Lorentzian wings of the resonance lines of the H_2O monomer could be significant. Note that the conclusion concerning an important contribution of stable dimers to the observed water vapor continuum is reminiscent of the analysis of the CO_2 spectra in the range of the Fermi doublet (1200–1500 cm^{-1}).[88]

7 Conclusions

The analysis of the observed continuum in the CO_2–CO_2 and CO_2–Ar molecular systems shows that it originates from the formation of pair molecular states in gas (bimolecular absorption). Qualitative and quantitative agreement between the experimental data and the results of CTS calculations (taking into account all possible pair states) allows us to state that, in the spectral range under consideration, the nature of the continuum of these gases has been established.

A comparative analysis of the CO_2–CO_2 and CO_2–Ar continua with the water vapor continuum indicates that there is much in common between them. In particular, in both cases, binary molecules (metastable and stable dimers) or simply dimers are responsible for most of the observed absorption. This part of the continuum cannot be modeled as non-Lorentzian wings of

Table 3 Uncertainty budget of spectral functions (in percent). The column "Others" includes uncertainties of gas temperature and pressure measurements, and uncertainties in determining the contribution of continuum absorption of water vapor

	CO_2–CO_2				CO_2–Ar			
		Others				Others		
T, K	Statistical	105–145 GHz	156–255 GHz	Final	Statistical	105–145 GHz	156–255 GHz	Final
268	1.42	0.89	1.12	**1.6**	3.21	2.32	2.98	**4.4**
279	1.08	0.84	0.71	**1.3**	2.21	2.15	2.70	**3.5**
297	1.05	1.07	0.54	**1.5**	2.67	2.27	3.25	**4.2**
317	1.34	1.33	1.07	**1.8**	3.11	2.41	1.70	**3.9**
332	1.56	—	0.87	**1.6**	—	—	—	—

monomer lines (as, *e.g.*, is assumed in the MT_CKD model[23]). As follows from our analysis, the non-Lorentzian wings of the resonance lines of the H_2O monomer (monomolecular absorption) make a significant contribution to the water vapor continuum. The lack of theoretical calculations of the spectra of metastable dimers and possible quantitative inaccuracies in the calculation of the spectrum of stable dimers do not allow us to speak in this case about the fully established nature of the continuum. In this regard, it is worth noting that the classical trajectories' method, in principle, allows solving the problem of the far wings of resonance lines, since it enables detailed monitoring of the evolution of the dipole moment of a monomer during collision.[89]

Conflicts of interest

There are no conflicts of interest to declare.

Appendix A: uncertainty budget for the spectral functions of the CO_2–CO_2 and CO_2–Ar continua

The statistical uncertainty was estimated as a standard deviation of the experimental points from the approximating function (4) fitted to them.

The error of the measured gas temperature was determined by the sensor error and the temperature gradient inside the chamber. The first component was known from the sensor specification (0.2 K); the second component was estimated as the difference between the average temperature and the arithmetic mean value for three available sensors. The uncertainty of the spectral functions associated with the error in the measured gas temperature was assessed based on the results of calculations of the temperature dependence of bimolecular absorption.[18,20]

The uncertainty of the obtained spectral functions was also associated with the inaccuracy of determining the concentration, so the gas pressure measurement error (precision of the pressure gauge) and gas temperature were taken into account.

The water vapor content in the studied sample was estimated using the 183-GHz H_2O line (integrated intensity 7.734×10^{-23} cm mol^{-1} [90]). In particular, if the line was not observed (the absorption at the line center was less than the experimental noise standard deviation), no correction was made. If the line was visible, then the water vapor pressure was estimated spectroscopically from the analysis of the observed profile.

The partial water vapor pressure was found to be less than 6 mTorr in all experimental records. The influence of the water vapor continuum (H_2O–CO_2) was taken into account based on the results of ref. 53, where the H_2O–CO_2 continuum was determined at a frequency of 239 GHz. It was assumed that the value of the H_2O–CO_2 continuum depends quadratically on frequency. This continuum component was subtracted from the observed absorption. A similar estimation was made for possible contribution of the H_2O–Ar continuum (based on the experimental data from ref. 53). This component was found to be negligibly small under the conditions of our experiments. The water vapor content uncertainty leads to an uncertainty of the H_2O–CO_2 continuum contribution and extends to the uncertainty of the studied spectra.

The resulting uncertainty of the spectral function, defined as the square root of the sum of all the listed uncertainties squared, was 1.6% and 5.9% for $S_{CO_2-CO_2}(f)$ and $S_{CO_2-Ar}(f)$, respectively. Note that the uncertainty of $S_{CO_2-Ar}(f)$ also included the uncertainty of $S_{CO_2-CO_2}(f)$.

The uncertainty of the spectral functions of CO_2–CO_2 and CO_2–Ar, determined in the 105–255 GHz frequency range in the temperature interval 268–332 K, was assessed in the same way as for the room temperature case. The resulting uncertainty of the spectral function was no more than 1.8% and 4.4% for $S_{CO_2-CO_2}(f)$ and $S_{CO_2-Ar}(f)$, respectively. Details of the uncertainty budget are summarized in Table 3.

Acknowledgements

The Russian Science Foundation (project no. 22-17-00041†) supported the study with the resonator spectrometer. The work was done using the research facilities CKP-7 (USU no. 3589084). The H_2O–H_2O continuum modeling is supported by the RSF project no. 22-72-10118.‡ The study of equilibrium constants and excluded volume was undertaken by DNC and AAV with partial support from the state assignment to the A.M. Obukhov Institute of Atmospheric Physics RAS (FMWR-2022-0010 and FMWR-2022-0016).

† https://rscf.ru/en/project/22-17-00041.
‡ https://rscf.ru/en/project/22-72-10118.

Notes and references

1 L. M. Trafton, in *Molecular complexes in Earth's, planetery, cometary and interstellar atmospheres*, ed. A. A. Vigasin and Z. Slanina, World Scientific, London, 1998, ch. 6, pp. 177–193.
2 R. Wordsworth, F. Forget and V. Eymet, *Icarus*, 2010, **210**, 992–997.
3 P. Jensen and P. R. Bunker, *Computational molecular spectroscopy*, Wiley, 2000, p. 688.
4 K. P. Shine, I. V. Ptashnik and G. Rädel, *Surv. Geophys.*, 2012, **33**, 535–555.
5 W. M. Elsasser, *Astrophys. J.*, 1938, **87**, 497.
6 D. E. Stogryn and J. O. Hirschfelder, *J. Chem. Phys.*, 1959, **31**, 1531–1545.
7 A. A. Vigasin, *Infrared Phys.*, 1991, **32**, 461–470.
8 A. A. Vigasin, in *Weakly interacting molecular pairs: Unconventional absorbers of radiation in the atmosphere*, ed. C. Camy-Peyret and A. A. Vigasin, Springer, 2003, pp. 23–47.
9 E. A. Serov, T. A. Odintsova, M. Yu. Tretyakov and V. E. Semenov, *J. Quant. Spectrosc. Radiat. Transfer*, 2017, **193**, 1–12.
10 T. Karman, E. Miliordos, K. L. C. Hunt, G. C. Groenenboom and A. van der Avoird, *J. Chem. Phys.*, 2015, **142**, 084306.
11 T. Karman, M. A. J. Koenis, A. Banerjee, D. H. Parker, I. E. Gordon, A. van der Avoird, W. J. van der Zande and G. C. Groenenboom, *Nat. Chem.*, 2018, **10**, 549–554.
12 J.-M. Hartmann, C. Boulet and D. Jacquemart, *J. Chem. Phys.*, 2011, **134**, 094316.
13 J.-M. Hartmann, C. Boulet and G. C. Toon, *J. Geophys. Res.: Atmos.*, 2017, **122**, 2419–2428.
14 W. Fakhardji, P. Szabó and M. Gustafsson, *J. Quant. Spectrosc. Radiat. Transfer*, 2021, **276**, 107926.
15 I. Buryak, L. Frommhold and A. A. Vigasin, *J. Chem. Phys.*, 2014, **140**, 154302.
16 D. V. Oparin, N. N. Filippov, I. M. Grigoriev and A. P. Kouzov, *J. Quant. Spectrosc. Radiat. Transfer*, 2017, **196**, 87–93.
17 D. N. Chistikov, A. A. Finenko, S. E. Lokshtanov, S. V. Petrov and A. A. Vigasin, *J. Chem. Phys.*, 2019, **151**, 194106.
18 D. N. Chistikov, A. A. Finenko, Yu. N. Kalugina, S. E. Lokshtanov, S. V. Petrov and A. A. Vigasin, *J. Chem. Phys.*, 2021, **155**, 064301.
19 E. A. Serov, A. A. Balashov, M. Yu. Tretyakov, T. A. Odintsova, M. A. Koshelev, D. N. Chistikov, A. A. Finenko, S. E. Lokshtanov, S. V. Petrov and A. A. Vigasin, *J. Quant. Spectrosc. Radiat. Transfer*, 2020, **242**, 106774.
20 T. A. Odintsova, E. A. Serov, A. A. Balashov, M. A. Koshelev, A. O. Koroleva, A. A. Simonova, M. Yu. Tretyakov, N. N. Filippov, D. N. Chistikov, A. A. Finenko, S. E. Lokshtanov, S. V. Petrov and A. A. Vigasin, *J. Quant. Spectrosc. Radiat. Transfer*, 2021, **258**, 107400.
21 A. A. Finenko, B. Bézard, I. E. Gordon, D. N. Chistikov, S. E. Lokshtanov, S. V. Petrov and A. A. Vigasin, *Astrophys. J., Suppl. Ser.*, 2022, **258**, 33.
22 L. Frommhold, *Collision induced absorption in gases*, Cambridge University Press, 2006.
23 E. J. Mlawer, V. H. Payne, J. L. Moncet, J. S. Delamere, M. J. Alvarado and D. C. Tobin, *Philos. Trans. R. Soc., A*, 2012, **370**, 2520–2556.
24 E. J. Mlawer, K. E. Cady-Pereira, J. Mascio and I. E. Gordon, *J. Quant. Spectrosc. Radiat. Transfer*, 2023, **306**, 108645.
25 T. A. Galanina, A. O. Koroleva, A. A. Simonova, A. Campargue and M. Yu. Tretyakov, *J. Mol. Spectrosc.*, 2022, **389**, 111691.
26 A. O. Koroleva, S. Kassi and A. Campargue, *J. Quant. Spectrosc. Radiat. Transfer*, 2022, **286**, 108206.
27 D. C. Catling, *Treatise on Geochemistry*, 2014, pp. 177–195.
28 J. F. Kasting, J. B. Pollack and D. Crisp, *J. Atmos. Chem.*, 1984, **1**, 403–428.
29 Yu. I. Baranov and A. A. Vigasin, *J. Mol. Spectrosc.*, 1999, **193**, 319–325.
30 Yu. I. Baranov, G. T. Fraser, W. J. Lafferty and A. A. Vigasin, in *Weakly interacting molecular pairs: Unconventional absorbers of radiation in the atmosphere*, ed. C. Camy-Peyret and A. A. Vigasin, Springer, 2003, pp. 149–158.
31 R. E. Asfin, J. V. Buldyreva, T. N. Sinyakova, D. V. Oparin and N. N. Filippov, *J. Chem. Phys.*, 2015, **142**, 051101.
32 M. Walsh, T. England, T. Dyke and B. Howard, *Chem. Phys. Lett.*, 1987, **142**, 265–270.
33 J. Norooz Oliaee, M. Dehghany, M. Rezaei, A. R. W. McKellar and N. Moazzen-Ahmadi, *J. Chem. Phys.*, 2016, **145**, 174302.
34 F. Huisken, L. Ramonat, J. Santos, V. Smirnov, O. Stelmakh and A. Vigasin, *J. Mol. Struct.*, 1997, **410**, 47–50.
35 Y. Scribano and C. Leforestier, *J. Chem. Phys.*, 2007, **126**, 234301.
36 E. Turner, S. Fox, V. Mattioli and D. Cimini, *Literature review on microwave and sub-millimetre spectroscopy for MetOp second generation*, EUMETSAT, NWPSAF-MO-TR-039, technical report, 2022.
37 Yu. I. Baranov, W. J. Lafferty, Q. Ma and R. H. Tipping, *J. Quant. Spectrosc. Radiat. Transfer*, 2008, **109**, 2291–2302.
38 Yu. I. Baranov and W. J. Lafferty, *J. Quant. Spectrosc. Radiat. Transfer*, 2011, **112**, 1304–1313.
39 I. V. Ptashnik, R. A. McPheat, K. P. Shine, K. M. Smith and R. G. Williams, *J. Geophys. Res.: Atmos.*, 2011, **116**, D16305.
40 I. V. Ptashnik, R. A. McPheat, K. P. Shine, K. M. Smith and R. G. Williams, *Philos. Trans. R. Soc., A*, 2012, **370**, 2557–2577.
41 I. V. Ptashnik, T. M. Petrova, Yu. N. Ponomarev, K. P. Shine, A. A. Solodov and A. M. Solodov, *J. Quant. Spectrosc. Radiat. Transfer*, 2013, **120**, 23–35.
42 I. V. Ptashnik, T. M. Petrova, Yu. N. Ponomarev, A. A. Solodov and A. M. Solodov, *Atmos. Oceanic Opt.*, 2015, **28**, 115–120.
43 D. E. Burch and R. L. Alt, *Continuum absorption by H_2O in the 700–1200 cm^{-1} and 2400–2800 cm^{-1} windows, Report AFGL-TR-84-0128*, Air Force Geophys. Laboratory, Hanscom AFB, MA, technical report, 1984.
44 D. Mondelain, S. Manigand, S. Kassi and A. Campargue, *J. Geophys. Res.: Atmos.*, 2014, **119**, 5625–5639.
45 D. Mondelain, S. Vasilchenko, P. Čermák, S. Kassi and A. Campargue, *Phys. Chem. Chem. Phys.*, 2015, **17**, 17762–17770.
46 A. Campargue, S. Kassi, D. Mondelain, S. Vasilchenko and D. Romanini, *J. Geophys. Res.: Atmos.*, 2016, **121**, 13180–13203.
47 M. A. Koshelev, I. I. Leonov, E. A. Serov, A. I. Chernova, A. A. Balashov, G. M. Bubnov, A. F. Andriyanov, A. P. Shkaev, V. V. Parshin, A. F. Krupnov and M. Yu. Tretyakov, *IEEE Trans. Terahertz Sci. Technol.*, 2018, **8**, 773–783.

48 M. Yu. Tretyakov, *High accuracy resonator spectroscopy of atmospheric gases at millimetre and submillimetre waves*, Cambridge Scholars Publishing, 2021.
49 I. R. Dagg, G. E. Reesor and J. L. Urbaniak, *Can. J. Phys.*, 1974, **52**, 973.
50 A. A. Maryott and S. J. Kryder, *J. Chem. Phys.*, 1964, **41**, 1580–1582.
51 I. R. Dagg, A. Anderson, S. Yan, W. Smith and C. G. Joslin, *Can. J. Phys.*, 1986, **64**, 1475.
52 W. Ho, G. Birnbaum and A. Rosenberg, *J. Chem. Phys.*, 1971, **55**, 1028–1038.
53 A. Bauer, M. Godon, J. Carlier and R. R. Gamache, *J. Mol. Spectrosc.*, 1996, **176**, 45–57.
54 L. Frenkel and D. Woods, *J. Chem. Phys.*, 1966, **44**, 2219.
55 I. R. Dagg, L. A. A. Read and J. Vanderkooy, *Rev. Sci. Instrum.*, 1982, **53**, 187–193.
56 R. Occelli, H. Blancher, G. Bachet and R. Coulon, *Int. J. Infrared Millimeter Waves*, 1987, **8**, 465–477.
57 I. R. Dagg, G. E. Reesor and M. Wong, *Can. J. Phys.*, 1978, **56**, 1037.
58 T. E. Sullivan and L. Frenkel, *J. Chem. Phys.*, 1970, **52**, 3847–3848.
59 A. A. Maryott and G. Birnbaum, *J. Chem. Phys.*, 1962, **36**, 2026–2032.
60 I. R. Dagg, G. E. Reesor and J. L. Urbaniak, *Can. J. Phys.*, 1975, **53**, 1764–1776.
61 H. Chen and J. C. Light, *J. Chem. Phys.*, 2000, **112**, 5070–5080.
62 S. E. Lokshtanov, S. V. Ivanov and A. A. Vigasin, *J. Mol. Struct.*, 2005, **742**, 31–36.
63 S. Y. Epifanov and A. A. Vigasin, *Mol. Phys.*, 1997, **90**, 101–106.
64 A. A. Vigasin, *J. Quant. Spectrosc. Radiat. Transfer*, 2014, **148**, 58–64.
65 I. Buryak and A. A. Vigasin, *J. Chem. Phys.*, 2015, **143**, 234304.
66 D. N. Chistikov, A. A. Finenko, S. E. Lokshtanov, S. V. Petrov and A. A. Vigasin, *J. Chem. Phys.*, 2018, **149**, 194304.
67 J. H. Dymond, K. N. Marsh, R. C. Wilhoit and K. C. Wong, *Virial coefficients of pure gases and mixtures*, Springer, London, England, 2002, vol. 21A,B.
68 M. Yu. Tretyakov, E. A. Serov and T. A. Odintsova, *Radiophys. Quantum Electron.*, 2012, **54**, 700–716.
69 C. Leforestier, *J. Chem. Phys.*, 2014, **140**, 074106.
70 T. A. Odintsova, M. Yu. Tretyakov, O. Pirali and P. Roy, *J. Quant. Spectrosc. Radiat. Transfer*, 2017, **187**, 116–123.
71 T. A. Odintsova, M. Yu. Tretyakov, A. O. Zibarova, O. Pirali, P. Roy and A. Campargue, *J. Quant. Spectrosc. Radiat. Transfer*, 2019, **227**, 190–200.
72 T. A. Odintsova, M. Yu. Tretyakov, A. A. Simonova, I. V. Ptashnik, O. Pirali and A. Campargue, *J. Mol. Struct.*, 2020, **1210**, 128046.
73 T. A. Odintsova, A. O. Koroleva, A. A. Simonova, A. Campargue and M. Yu. Tretyakov, *J. Mol. Spectrosc.*, 2022, **386**, 111603.
74 T. Kuhn, A. Bauer, M. Godon, S. Bühler and K. Künzi, *J. Quant. Spectrosc. Radiat. Transfer*, 2002, **74**, 545–562.
75 V. B. Podobedov, D. F. Plusquellic, K. E. Siegrist, G. T. Fraser, Q. Ma and R. H. Tipping, *J. Quant. Spectrosc. Radiat. Transfer*, 2008, **109**, 458–467.
76 M. A. Koshelev, E. A. Serov, V. V. Parshin and M. Yu. Tretyakov, *J. Quant. Spectrosc. Radiat. Transfer*, 2011, **112**, 2704–2712.
77 M. Yu. Tretyakov, E. A. Serov, M. A. Koshelev, V. V. Parshin and A. F. Krupnov, *Phys. Rev. Lett.*, 2013, **110**, 093001.
78 E. A. Serov, M. A. Koshelev, T. A. Odintsova, V. V. Parshin and M. Yu. Tretyakov, *Phys. Chem. Chem. Phys.*, 2014, **16**, 26221–26233.
79 D. E. Burch, *Continuum absorption by H_2O*, AFGL, No. 81-0300 technical report, 1982.
80 D. M. Slocum, R. H. Giles and T. M. Goyette, *J. Quant. Spectrosc. Radiat. Transfer*, 2015, **159**, 69–79.
81 H. J. Liebe and D. H. Layton, *Millimeter-wave properties of the atmosphere: Laboratory studies and propagation modeling*, NTIA 87-224 technical report, 1987.
82 V. Yu. Katkov, B. A. Sverdlov and N. I. Furashov, *Radiophys. Quantum Electron.*, 1995, **36**, 835–844.
83 M. Yu. Tretyakov, A. A. Sysoev, T. A. Odintsova and A. A. Kyuberis, *Radiophys. Quantum Electron.*, 2015, **58**, 262–276.
84 Q. Ma, C. Boulet and R. H. Tipping, *J. Chem. Phys.*, 2014, **140**, 244301.
85 A. Vigasin, *Mol. Phys.*, 2010, **108**, 2309–2313.
86 G. T. Fraser, R. D. Suenram and L. H. Coudert, *J. Chem. Phys.*, 1989, **90**, 6077–6085.
87 B. E. Rocher-Casterline, L. C. Ch'ng, A. K. Mollner and H. Reisler, *J. Chem. Phys.*, 2011, **134**, 211101.
88 A. A. Vigasin, Yu. I. Baranov and G. V. Chlenova, *J. Mol. Spectrosc.*, 2002, **213**, 51–56.
89 S. V. Ivanov, *J. Quant. Spectrosc. Radiat. Transfer*, 2016, **177**, 269–282.
90 I. E. Gordon, L. S. Rothman, R. J. Hargreaves, R. Hashemi, E. V. Karlovets, F. M. Skinner, E. K. Conway, C. Hill, R. V. Kochanov, Y. Tan, P. Wcisło, A. A. Finenko, K. Nelson, P. F. Bernath, M. Birk, V. Boudon, A. Campargue, K. V. Chance, A. Coustenis, B. J. Drouin, J. M. Flaud, R. R. Gamache, J. T. Hodges, D. Jacquemart, E. J. Mlawer, A. V. Nikitin, V. I. Perevalov, M. Rotger, J. Tennyson, G. C. Toon, H. Tran, V. G. Tyuterev, E. M. Adkins, A. Baker, A. Barbe, E. Canè, A. G. Császár, A. Dudaryonok, O. Egorov, A. J. Fleisher, H. Fleurbaey, A. Foltynowicz, T. Furtenbacher, J. J. Harrison, J. M. Hartmann, V. M. Horneman, X. Huang, T. Karman, J. Karns, S. Kassi, I. Kleiner, V. Kofman, F. Kwabia-Tchana, N. N. Lavrentieva, T. J. Lee, D. A. Long, A. A. Lukashevskaya, O. M. Lyulin, V. Y. Makhnev, W. Matt, S. T. Massie, M. Melosso, S. N. Mikhailenko, D. Mondelain, H. S. P. Müller, O. V. Naumenko, A. Perrin, O. L. Polyansky, E. Raddaoui, P. L. Raston, Z. D. Reed, M. Rey, C. Richard, R. Tóbiás, I. Sadiek, D. W. Schwenke, E. Starikova, K. Sung, F. Tamassia, S. A. Tashkun, J. Vander Auwera, I. A. Vasilenko, A. A. Vigasin, G. L. Villanueva, B. Vispoel, G. Wagner, A. Yachmenev and S. N. Yurchenko, *J. Quant. Spectrosc. Radiat. Transfer*, 2022, **277**, 107949.